Computer Methods in Applied Mechanics and Engineering 461 (2026) 119199

Contents lists available at ScienceDirect

Comput. Methods Appl. Mech. Engrg.

journal homepage: www.elsevier.com/locate/cma

Exact operator inference decouples parametric problems

Henrik Rosenberger [a,b,*], Benjamin Sanderse [a,b], Giovanni Stabile [c]

[a] Centrum Wiskunde & Informatica, Amsterdam, The Netherlands
[b] Centre for Analysis, Scientific Computing and Applications, Eindhoven University of Technology, Eindhoven, The Netherlands
[c] The Biorobotics Institute, Sant'Anna School of Advanced Studies, Pisa, Italy

ARTICLE INFO

Keywords:
Non-intrusive model reduction
Parametric model reduction
Data-driven modeling
Operator inference
Decoupling

ABSTRACT

The application of operator inference to parametric problems whose operators exhibit affine parameter dependency results in a minimization problem with three issues. First, the solution to the minimization problem is generally not unique, so we might obtain a different solution than the one we are interested in. Second, time discretization inconsistencies and non-Markovian information can cause errors in the inferred operators. Third, the large dimensions of the minimization problem can cause prohibitively high computational costs. In this work, we resolve these issues by extending previous work on exact operator inference to the parametric case. Concretely, we propose a snapshot data generation method that guarantees the uniqueness of the solution and the absence of time discretization inconsistencies and non-Markovian information, and thereby the exact reconstruction of the corresponding intrusive operators of projection-based reduced order models. Furthermore, we show that the monolithic problem that comprises the snapshot data of all sampled parameters can be decoupled into separate problems for only one parameter sample each. This decoupling results in smaller subproblems that are embarrassingly parallel, numerically more stable and can be solved more efficiently. In numerical experiments, we demonstrate this decoupling for the heat equation with two different temperature-, parameter- and space-dependent thermal conductivities.

1. Introduction

The aim of model reduction is to reduce the computational cost of numerical simulations in complex engineering tasks such as optimization, data assimilation, uncertainty quantification and the development of digital twins. All these tasks involve multiple simulations that depend on variable parameters.

In this work we consider problems described by a dynamical system with parameter-dependent right-hand side. Such dynamical systems are, for example, derived from spatial discretizations of PDEs with parameter-dependent geometries or physical properties. Other types of parameter-dependency considered in other works include parametric initial conditions [1,2] and parametric inputs such as boundary conditions [3].

In intrusive projection-based model reduction, parameter dependencies in the operators of the high-fidelity model are directly inherited by the reduced-order model (ROM) [4]. However, intrusive model reduction is often not feasible in practice because it requires access to numerical operators that is not possible in industry software. To address this practical problem, nonintrusive model reduction constructs ROMs without intrusive software access but only based on output data of the high-fidelity simulations. In particular, operator inference aims at reproducing the same ROMs as intrusive projection-based model reduction but nonintrusively [5,6]. Based on snapshot data of high-fidelity simulations, ROM operators of given polynomial degree are computed as

* Corresponding author at: Centrum Wiskunde & Informatica, Amsterdam, The Netherlands.
E-mail addresses: henrik.rosenberger@cwi.nl (H. Rosenberger), sanderse@cwi.nl (B. Sanderse), giovanni.stabile@santannapisa.it (G. Stabile).

https://doi.org/10.1016/j.cma.2026.119199
Received 9 April 2026; Received in revised form 24 June 2026; Accepted 24 June 2026
Available online 1 July 2026

solution to a minimization problem. However, in context of parameter-dependent problems [7–11], operator inference has three issues. First, the solution to the minimization problem is not unique if the provided snapshot data is not informative enough. In that case the computed solution can be very different to the intrusive ROM operators that we are interested in. Second, time discretization inconsistencies and non-Markovian information in the snapshot data can introduce errors in the inferred operators. This issue has been resolved in [12] via a method known as re-projection that guarantees exact reconstruction if the first issue does not take effect. Third, solving the minimization problem can cause prohibitively high computational costs because of the large dimensions of this problem. These dimensions depend on the complexity of the parameter dependency, the polynomial degree of the underlying problem and the considered ROM dimension. If these quantities are sufficiently large, the computational costs of the minimization problem can even dominate the overall offline costs of the ROM.

In this work, we resolve all three issues by extending previous work on non-parametric operator inference [13] to the parametric case. Concretely, we propose a snapshot data generation method that guarantees the uniqueness of the solution to the minimization problem and avoids time discretization inconsistencies and non-Markovian information in the snapshot data. As a consequence, the computed solution is an exact reconstruction of the intrusive ROM operators up to machine precision. Moreover, we show that for this snapshot data the minimization problem simplifies to a linear system that decouples into smaller linear systems. As a result, the computational costs are significantly smaller. In addition, the decoupled linear systems have a smaller condition number and can be solved in parallel.

This article is organized as follows. In Section 2, we introduce parametric dynamical systems, intrusive and non-intrusive projection-based model reduction and non-parametric exact operator inference. In Section 3 we extend exact operator inference to the parametric case. In Section 4 we describe the decoupling resulting from this extension. In Section 5 we present an alternative derivation for the same decoupling method. In Section 6 we present numerical experiments for the heat equation with different thermal conductivities. Finally, in Section 7 we draw conclusions.

2. Preliminaries

2.1. Parametric dynamical system

We consider the dynamical system of dimension N,

$$\dot{\boldsymbol{x}}(t;\boldsymbol{\mu}) = \boldsymbol{f}\left(\boldsymbol{x}(t;\boldsymbol{\mu});\boldsymbol{\mu}\right), \quad \boldsymbol{x}(0;\boldsymbol{\mu}) = \boldsymbol{x}_0(\boldsymbol{\mu}), \tag{1}$$

parametrized by $\boldsymbol{\mu} \in \mathcal{D} \subset \mathbb{R}^d$. We assume that the function $\boldsymbol{f} : \mathbb{R}^N \times \mathcal{D} \to \mathbb{R}^N$ has polynomial structure, and for ease of presentation, we assume a quadratic term here,

$$\boldsymbol{f}\left(\boldsymbol{x};\boldsymbol{\mu}\right) = \mathbf{H}(\boldsymbol{\mu})\boldsymbol{x}^2, \tag{2}$$

where $\boldsymbol{x}^2 \in \mathbb{R}^{\binom{N+1}{2}}$ comprises all unique products of two entries of $\boldsymbol{x}$ as described in [12,13] and $\mathbf{H} : \mathcal{D} \to \mathbb{R}^{N\times\binom{N+1}{2}}$. Functions $\boldsymbol{f}$ that are monomials in $\boldsymbol{x}$ of any other order can be handled analogously. Functions $\boldsymbol{f}$ that are sums of multiple monomial terms are discussed in Appendix A.

2.2. Parametric Galerkin ROM

To obtain a Galerkin ROM, the FOM is projected onto a basis $\mathbf{V}_n \in \mathbb{R}^{N\times n}$, $n \ll N$, and the FOM state $\boldsymbol{x}(t;\boldsymbol{\mu})$ is replaced by a lower dimensional approximation $\mathbf{V}_n\tilde{\boldsymbol{x}}(t;\boldsymbol{\mu})$,

$$\dot{\tilde{\boldsymbol{x}}}(t;\boldsymbol{\mu}) = \tilde{\mathbf{H}}(\boldsymbol{\mu})\tilde{\boldsymbol{x}}^2(t;\boldsymbol{\mu}) \tag{3}$$

with the ROM state $\tilde{\boldsymbol{x}}(t;\boldsymbol{\mu}) \in \mathbb{R}^n$ and the projected matrix defined by

$$\tilde{\mathbf{H}}(\boldsymbol{\mu}) = \mathbf{V}_n^T\mathbf{H}(\boldsymbol{\mu})\mathbf{I}_N^{(i)}\left(\mathbf{V}_n \otimes \mathbf{V}_n\right)\mathbf{J}_n^{(i)}, \tag{4}$$

with matrices $\mathbf{I}_N^{(i)} \in \{0,1\}^{\binom{N+1}{2}\times N^2}$ and $\mathbf{J}_n^{(i)} \in \{0,1\}^{n^2\times\binom{n+1}{2}}$ as described in [12].

There are several methods to define the basis $\mathbf{V}_n$ [4]. In this work, we consider a global basis obtained from POD of snapshots $[\mathbf{X}(\bar{\boldsymbol{\mu}}_1) \ \ldots \ \mathbf{X}(\bar{\boldsymbol{\mu}}_{s_{\text{POD}}})]$ with

$$\mathbf{X}(\bar{\boldsymbol{\mu}}_i) := [\boldsymbol{x}(\bar{t}_1;\bar{\boldsymbol{\mu}}_i) \ \ldots \ \boldsymbol{x}(\bar{t}_{K_{\text{POD}}};\bar{\boldsymbol{\mu}}_i)] \in \mathbb{R}^{N\times K_{\text{POD}}}$$

at sampled parameters $\bar{\boldsymbol{\mu}}_1, \ldots, \bar{\boldsymbol{\mu}}_{s_{\text{POD}}} \in \mathcal{D}$ with $K_{\text{POD}}, s_{\text{POD}} \in \mathbb{N}$. How to choose such parameter samples is discussed in [4].

Computing ROM operators for new parameter values $\boldsymbol{\mu}$ via (4) is not efficient because the computational costs scale with the FOM dimension N. Instead, we assume that the FOM operator can be affinely decomposed,

$$\mathbf{H}(\boldsymbol{\mu}) = \sum_{p=1}^{q_H} \theta_H^{(p)}(\boldsymbol{\mu})\mathbf{H}^{(p)}, \tag{5}$$

with scalar functions $\theta_H^{(p)} : \mathcal{D} \to \mathbb{R}$ and matrices $\mathbf{H}^{(p)} \in \mathbb{R}^{N\times\binom{N+1}{2}}$, $p = 1, \ldots, q_H$. Then, we can precompute

$$\tilde{\mathbf{H}}^{(p)} = \mathbf{V}_n^T\mathbf{H}^{(p)}\mathbf{I}_N^{(i)}\left(\mathbf{V}_n \otimes \mathbf{V}_n\right)\mathbf{J}_n^{(i)}, \quad p = 1, \ldots, q_H, \tag{6}$$

during the offline phase, and compute

$$\tilde{\mathbf{H}}(\boldsymbol{\mu}) = \sum_{p=1}^{q_H} \theta_H^{(p)}(\boldsymbol{\mu})\tilde{\mathbf{H}}^{(p)} \tag{7}$$

efficiently during the online phase with computational costs only depending on the ROM dimension n. However, the computations (6) are intrusive since they require access to the FOM operator components $\mathbf{H}^{(r)}$. As a non-intrusive alternative, our goal is to infer the ROM operator components $\tilde{\mathbf{H}}^{(r)}$ from data in the next section.

Note that not all parametric FOM operators possess an affine structure of the form (5) with known coefficient functions $\theta_H^{(p)} : \mathcal{D} \to \mathbb{R}$. However, operators without this structure can still be approximated by such affine expansions. For example, Taylor approximations [14], interpolation [15] and hyperreduction techniques such as DEIM [4] and GNAT [16] have been used in the context of intrusive model reduction. These hyperreduction techniques are based on the assumption that single entries of operators can be computed more efficiently than the complete operators. Non-intrusive model reduction, however, does not directly access operators at all, so hyperreduction techniques are not applicable. In the non-intrusive context of operator inference, affine expansions have been considered that describe the parameter dependency exactly [7,8] or are derived from Taylor approximations [10] and piecewise-linear interpolation [17]. All these approximations introduce errors and can suffer from the curse of dimensionality if $\boldsymbol{\mu}$ is high-dimensional, so achieving satisfactory accuracy can be challenging [4].

2.3. Parametric operator inference

As in the non-parametric case, operator inference with affine parameter dependency uses two sets of snapshot data. The first one to generate the ROM basis, the second one to infer the operators. These two sets can comprise different snapshots; in particular, parameter samples the $\boldsymbol{\mu}_1, \dots, \boldsymbol{\mu}_s \in \mathcal{D}$ corresponding to the second set can be different from the parameter samples $\bar{\boldsymbol{\mu}}_1, \dots, \bar{\boldsymbol{\mu}}_{s_{\text{POD}}}$ corresponding to the first set, as described in the previous subsection. Let

$$\mathbf{X}(\boldsymbol{\mu}_i) := \begin{bmatrix} \boldsymbol{x}(t_1;\boldsymbol{\mu}_i) & \dots & \boldsymbol{x}(t_K;\boldsymbol{\mu}_i) \end{bmatrix} \in \mathbb{R}^{N\times K},\ i = 1, \dots, s \tag{8}$$

be this second set of snapshots with the corresponding time derivative snapshots

$$\dot{\mathbf{X}}(\boldsymbol{\mu}_i) := \begin{bmatrix} \frac{\mathrm{d}}{\mathrm{d}t}\boldsymbol{x}(t_1;\boldsymbol{\mu}_i) & \dots & \frac{\mathrm{d}}{\mathrm{d}t}\boldsymbol{x}(t_K;\boldsymbol{\mu}_i) \end{bmatrix} \in \mathbb{R}^{N\times K},\ i = 1, \dots, s, \tag{9}$$

with $K, s \in \mathbb{N}$ not necessarily equal to K_{POD} and s_{POD}, respectively.

As described in [7,9], the operator inference problem to infer the operator matrix

$$\hat{\mathbf{O}} := \begin{bmatrix} \hat{\mathbf{H}}^{(1)} & \dots & \hat{\mathbf{H}}^{(q_H)} \end{bmatrix} \in \mathbb{R}^{n\times q(n)},\ q(n) = q_H\binom{n+1}{2} \tag{10}$$

from the projected snapshot data

$$\hat{\mathbf{X}}(\boldsymbol{\mu}_i) = \mathbf{V}^T\mathbf{X}(\boldsymbol{\mu}_i), \quad i = 1, \dots, s, \tag{11}$$

$$\dot{\hat{\mathbf{X}}}(\boldsymbol{\mu}_i) = \mathbf{V}^T\dot{\mathbf{X}}(\boldsymbol{\mu}_i), \quad i = 1, \dots, s, \tag{12}$$

is to minimize

$$\mathcal{L}(\hat{\mathbf{O}}) := \sum_{i=1}^{s} \left\| \hat{\mathbf{X}}_2(\boldsymbol{\mu}_i)^T \left[\sum_{p=1}^{q_H} \theta_H^{(p)}(\boldsymbol{\mu}_i)\hat{\mathbf{H}}^{(p)} \right]^T - \dot{\hat{\mathbf{X}}}(\boldsymbol{\mu}_i)^T \right\|_F^2 \tag{13}$$

$$= \left\| \mathbf{D}\hat{\mathbf{O}}^T - \mathbf{R}^T \right\|_F^2. \tag{14}$$

with the matrices $\mathbf{R} = \begin{bmatrix} \dot{\hat{\mathbf{X}}}(\boldsymbol{\mu}_1) & \dots & \dot{\hat{\mathbf{X}}}(\boldsymbol{\mu}_s) \end{bmatrix} \in \mathbb{R}^{n\times sK}$ and

$$\mathbf{D} := \begin{bmatrix} \boldsymbol{\theta}_H(\boldsymbol{\mu}_1) \otimes \hat{\mathbf{X}}_2(\boldsymbol{\mu}_1)^T \\ \vdots \\ \boldsymbol{\theta}_H(\boldsymbol{\mu}_s) \otimes \hat{\mathbf{X}}_2(\boldsymbol{\mu}_s)^T \end{bmatrix} \in \mathbb{R}^{sK\times q_H\binom{n+1}{2}}, \tag{15}$$

with

$$\boldsymbol{\theta}_H(\boldsymbol{\mu}_i) = \begin{bmatrix} \theta_H^{(1)}(\boldsymbol{\mu}_i) & \dots & \theta_H^{(q_H)}(\boldsymbol{\mu}_i) \end{bmatrix} \in \mathbb{R}^{1\times q_H},\ i = 1, \dots, s, \tag{16}$$

and

$$\hat{\mathbf{X}}_2(\boldsymbol{\mu}_i) := \begin{bmatrix} \hat{\boldsymbol{x}}^2(t_1;\boldsymbol{\mu}_i) & \dots & \hat{\boldsymbol{x}}^2(t_K;\boldsymbol{\mu}_i) \end{bmatrix} \in \mathbb{R}^{\binom{n+1}{2}\times K}. \tag{17}$$

There are three issues with the operator inference problem of minimizing (14): First, the uniqueness of the solution to this minimization problem is generally not guaranteed. Consequently, we might obtain a different solution than the one we are interested in. Second, time discretization inconsistencies and non-Markovian information in the snapshot data can introduce errors in the inferred operators. Both issues have been addressed by us in [13] in the context of non-parametric operator inference. In the next subsection, we will summarize that work and in Section 3 we will show how it can be generalized to the parametric case. Third, this

minimization problem has very large dimensions. These large dimensions cause high computational costs and can affect numerical stability [9]. In detail, the matrix $\mathbf{D}$ has column dimension $q_H\binom{n+1}{2}$ or more generally a column dimension of $\mathcal{O}(q_l n^l)$ with l the largest polynomial degree in the right-hand side $\boldsymbol{f}$ in (1) and q_l the number of terms in the affine decomposition analogous to (5) of the operator with this highest polynomial degree l. The computational cost of solving the least squares problem scales cubically in this column dimension of $\mathbf{D}$, so $\mathcal{O}((q_l n^l)^3)$. These costs can contribute substantially to the offline preparation of the ROM, even though they do not depend on the FOM dimension N. Moreover, the computational costs can be even larger when the linear least squares problem (14) is extended by constraints [18–20] or replaced by a nonlinear optimization problem [21] in order to preserve structure. The large dimensions are a consequence of comprising all affine operators $\hat{\mathbf{H}}^{(i)}$ and the snapshot data for all parameter samples $\boldsymbol{\mu}_i$ in one single optimization problem. In contrast, in intrusive model reduction, the affine operators $\tilde{\mathbf{H}}^{(i)}$ can be computed separately as described in (6). To achieve a similar separation with non-intrusive operator inference, we present in Section 4 a strategy to decouple the monolithic optimization problem (14) into smaller subproblems that only pertain one affine operator $\hat{\mathbf{H}}^{(i)}$ each. These smaller problems can be solved embarrassingly parallel and have a smaller condition number and are hence numerically more stable.

2.4. Exact operator inference

In [13], we have proposed a method to generate snapshot data for operator inference that guarantees exact reconstruction in the non-parametric case. This method has two key steps: First we identify ROM states that ensure the full rank of the operator inference least squares matrix. This identification is done based on the polynomial terms contained in the right-hand side $\boldsymbol{f}$ in (1). In the purely quadratic case (2) considered here, such a set of ROM states is given by the set of all sums of two unit vectors in $\mathbb{R}^n$,

$$\mathcal{X}^2 := \{\boldsymbol{e}_i + \boldsymbol{e}_j \mid \quad \boldsymbol{e}_i, \boldsymbol{e}_j \in \mathbb{R}^n \ \text{ unit vectors}\}. \tag{18}$$

Let $\hat{\boldsymbol{x}}_j \in \mathcal{X}^2$, $j = 1, \dots, \binom{n+1}{2}$ be the $\binom{n+1}{2}$ distinct elements of $\mathcal{X}^2$, then the matrix

$$\hat{\mathbf{X}}_2 := \begin{bmatrix} \hat{\boldsymbol{x}}_1^2 & \dots & \hat{\boldsymbol{x}}_{\binom{n+1}{2}}^2 \end{bmatrix} \in \mathbb{R}^{\binom{n+1}{2} \times \binom{n+1}{2}} \tag{19}$$

has full rank.

To generate the matrix $\dot{\hat{\mathbf{X}}}$ of corresponding ROM state time derivative snapshots, the second key step is to perform $\binom{n+1}{2}$ FOM simulations each for only a single time step. The initial conditions of these simulations are the FOM states corresponding to the identified ROM states $\hat{\boldsymbol{x}}_j$.

The snapshot data generated by this method is equivalent to snapshot data that one would obtain from simulating the corresponding intrusive ROM. Consequently, the intrusive ROM operator is a solution to the operator inference least squares problems. Since the matrix $\hat{\mathbf{X}}_2$ has full rank, this solution is unique, so operator inference exactly reconstructs the intrusive ROM operators.

The complete snapshot data generation method is summarized in Algorithm 1. In exact arithmetics, the time step size Δt is irrelevant for the resulting matrices $\hat{\mathbf{X}}_2$ and $\dot{\hat{\mathbf{X}}}$. In practice, however, Δt should be chosen to enable accurate floating-point number representations as explained in more detail in [13].

Algorithm 1 Exact operator inference snapshot data generation [13]

procedure exactOpInfSnapshots(
ROM basis $\mathbf{V}_n \in \mathbb{R}^{N \times n}$,
time step size Δt
)
  Initialize $\hat{\mathbf{X}}_2 \leftarrow \emptyset$
  Initialize $\dot{\hat{\mathbf{X}}} \leftarrow \emptyset$
  for $\hat{\boldsymbol{x}} \in \mathcal{X}^2$ **do**
    $\boldsymbol{x}_0 \leftarrow \mathbf{V}_n \hat{\boldsymbol{x}}$
    $\boldsymbol{x}_1 \leftarrow$ FOM(initial condition $\boldsymbol{x}_0$,
      time step size Δt, end time $T = \Delta t$, explicit Euler time discretization)
    $\hat{\mathbf{X}}_2 \leftarrow \hat{\boldsymbol{x}}^2$
    $\dot{\hat{\mathbf{X}}} \leftarrow [\dot{\hat{\mathbf{X}}}, \ \frac{\mathbf{V}_n^T \boldsymbol{x}_1 - \hat{\boldsymbol{x}}}{\Delta t}]$
  end for
  return $\hat{\mathbf{X}}_2$, $\dot{\hat{\mathbf{X}}}$
end procedure

3. Exact parametric operator inference

In this section we address the issue of non-unique solutions to the parametric operator inference least squares problem defined by (14). This problem has a unique solution if the matrix $\mathbf{D}$ has full column rank. As described in Theorem 2.3 in [7], $\mathbf{D}$ has full column rank if the matrix $\boldsymbol{\Theta}_H \in \mathbb{R}^{s \times q_H}$ defined by

$$\left[\boldsymbol{\Theta}_H\right]_{ij} = \theta_H^{(j)}(\boldsymbol{\mu}_i), \tag{20}$$

and all $\widehat{\mathbf{X}}_2(\boldsymbol{\mu}_i)$, $i = 1, \ldots, s$ have full column rank.

The first novelty of this work is a snapshot data generation method that guarantees full rank of the matrices $\widehat{\mathbf{X}}_2(\boldsymbol{\mu}_i)$, $i = 1, \ldots, s$. For this purpose we use the exact non-parametric operator inference snapshot data generation method described in Section 2.4 and extend it to the parametric case. In detail, we run Algorithm 1 for each parameter sample $\boldsymbol{\mu}_i$ to obtain the outputs $\widehat{\mathbf{X}}_2(\boldsymbol{\mu}_i)$ and $\dot{\widehat{\mathbf{X}}}(\boldsymbol{\mu}_i)$ as summarized in Algorithm 2. Note that the matrices $\widehat{\mathbf{X}}_2(\boldsymbol{\mu}_i)$ are actually not affected by the parameter $\boldsymbol{\mu}_i$ but equal to the matrix $\widehat{\mathbf{X}}_2$ resulting from the non-parametric Algorithm 1. In particular these matrices all have full column rank.

Algorithm 2 Exact parametric operator inference snapshot data generation

procedure exactParametricOpInfSnapshots(
ROM basis $\mathbf{V}_n \in \mathbb{R}^{N\times n}$,
time step size Δt
parameter samples $\boldsymbol{\mu}_1, \ldots, \boldsymbol{\mu}_s$
)
  for $\boldsymbol{\mu}_i = \boldsymbol{\mu}_1, \ldots, \boldsymbol{\mu}_s$ **do**
    Initialize $\widehat{\mathbf{X}}_2(\boldsymbol{\mu}_i) \leftarrow \emptyset$
    Initialize $\dot{\widehat{\mathbf{X}}}(\boldsymbol{\mu}_i) \leftarrow \emptyset$
    for $\widehat{\boldsymbol{x}} \in \mathcal{X}^2$ **do**
      $\boldsymbol{x}_0 \leftarrow \mathbf{V}_n\widehat{\boldsymbol{x}}$
      $\boldsymbol{x}_1 \leftarrow$ FOM(initial condition $\boldsymbol{x}_0$,
        time step size Δt, end time $T = \Delta t$, explicit Euler time discretization
        parameter $\boldsymbol{\mu}_i$)
      $\widehat{\mathbf{X}}_2(\boldsymbol{\mu}_i) \leftarrow \widehat{\boldsymbol{x}}^2$
      $\dot{\widehat{\mathbf{X}}}(\boldsymbol{\mu}_i) \leftarrow [\dot{\widehat{\mathbf{X}}}(\boldsymbol{\mu}_i), \ \frac{\mathbf{V}_n^T\boldsymbol{x}_1 - \widehat{\boldsymbol{x}}}{\Delta t}]$
    end for
  end for
  return $\left(\widehat{\mathbf{X}}_2(\boldsymbol{\mu}_1), \dot{\widehat{\mathbf{X}}}(\boldsymbol{\mu}_1)\right), \ldots, \left(\widehat{\mathbf{X}}_2(\boldsymbol{\mu}_s), \dot{\widehat{\mathbf{X}}}(\boldsymbol{\mu}_s)\right)$
end procedure

On the other hand, ensuring full column rank of $\boldsymbol{\Theta}_H$ is highly problem-specific. In view of the definitions of the functions $\theta_H^{(j)}$, parameter samples $\boldsymbol{\mu}_i$ must be chosen to achieve this full rank. In general, it is unclear how such parameter samples can be found; this is beyond the scope of this article. However, for polynomial functions $\theta_H^{(j)}$ that arise for example from Taylor approximations as described in [10], full-rank-ensuring parameter samples can be identified analogously to the full-rank-ensuring ROM states in [13].

If $\boldsymbol{\Theta}_H$ indeed has full column rank and the parameter dependency of the operator $\widehat{\mathbf{H}}$ can be expressed exactly by an affine expansion such as (5), then the snapshot data generated proposed in [13] ensures that the parametric operator inference exactly reconstructs the intrusive ROM operators. Furthermore, for any full column rank matrix $\boldsymbol{\Theta}_H \in \mathbb{R}^{s\times q_H}$ with $s > q_H$, there exists a subset of q_H rows that also form a matrix with full column rank q_H. These rows correspond to q_H of the s parameter samples $\boldsymbol{\mu}_i$, $i = 1, \ldots, s$. In the following, we can therefore assume that $s = q_H$ parameter samples are used.

Additionally, as described in [13], Algorithm 1 does not introduce time discretization inconsistencies or non-Markovian information in the snapshot data. This property is preserved by Algorithm 2, so the generated snapshots guarantee that the solution to the parametric operator inference problem (14) reconstructs the intrusive ROM operators exactly. The following section describes how the computational costs of solving this problem can be reduced significantly via decoupling.

4. Decoupling of exact parametric operator inference

The parametric operator inference minimization problem (14) is high-dimensional because it involves data from $s = q_H$ parameter samples to learn q_H quadratic operators. We want to decouple this problem into q_H subproblems that each only involve data from a single parameter sample to learn a single quadratic operator. For this purpose, we first note that if $\boldsymbol{\Theta}_H$ is the s-dimensional identity matrix $\mathbf{I}_s$, then the objective function (13) simplifies to

$$\mathcal{L}(\widehat{\mathbf{O}}) = \sum_{i=1}^{s} \left\| \widehat{\mathbf{X}}_2(\boldsymbol{\mu}_i)^T \left[\theta_H^{(i)}(\boldsymbol{\mu}_i)\widehat{\mathbf{H}}^{(i)}\right]^T - \dot{\widehat{\mathbf{X}}}(\boldsymbol{\mu}_i)^T \right\|_F^2, \tag{21}$$

so for all $i = 1, \ldots, s$, the operator $\widehat{\mathbf{H}}^{(i)}$ only depends on data from the parameter sample $\boldsymbol{\mu}_i$. Hence, one can solve subproblems for the basis operators $\widehat{\mathbf{H}}^{(i)}$ separately,

$$\widehat{\mathbf{H}}^{(i)} = \min_{\widehat{\mathbf{H}}^{(i)}} \left\| \widehat{\mathbf{X}}_2(\boldsymbol{\mu}_i)^T \left[\theta_H^{(i)}(\boldsymbol{\mu}_i)\widehat{\mathbf{H}}^{(i)}\right]^T - \dot{\widehat{\mathbf{X}}}(\boldsymbol{\mu}_i)^T \right\|_F^2, \quad i = 1, \ldots, q_H \tag{22}$$

In general, however, the condition $\Theta_H = \mathbf{I}_s$ does not hold. There are special cases such as in [17] where the condition $\Theta_H = \mathbf{I}_s$ is implicitly satisfied because the parameter dependency of a linear operator is approximated by piecewise-linear interpolation of the operator evaluated at parameter samples. In other cases, parameter samples $\boldsymbol{\mu}_i$ might exists such that $\Theta_H = \mathbf{I}_s$ as well. However, for most affine expansions (5) such parameter samples do not exist, or are not physical, so corresponding snapshot data cannot be generated. In the following, we therefore propose a decoupling method for general square matrices $\boldsymbol{\Theta}_H$ with full rank.

This decoupling method is based on two key insights. The first key insight is that the least squares problem defined by (14) can be simplified to a linear system analogously to the non-parametric case in [13]. For this purpose, we first note that this least squares problem is equivalent to the normal equations

$$\mathbf{D}^T\mathbf{D}\hat{\mathbf{O}}^T = \mathbf{D}^T\mathbf{R}^T. \tag{23}$$

As described in Section 3, the matrix $\mathbf{D}$ has full rank if the matrices $\hat{\mathbf{X}}_2(\boldsymbol{\mu}_i)$ are obtained from Algorithm 2 with suitable parameter samples $\boldsymbol{\mu}_i$, $i = 1, \dots, s$. If additionally $s = q_H$, then $\mathbf{D}$ is also square and the normal equations simplify to

$$\mathbf{D}\hat{\mathbf{O}}^T = \mathbf{R}^T. \tag{24}$$

The second key insight of our method is that, as described in Section 3, the matrices $\hat{\mathbf{X}}_2(\boldsymbol{\mu}_i)$ resulting from Algorithm 2 are actually independent of the parameter $\boldsymbol{\mu}_i$ and equal to the matrix $\hat{\mathbf{X}}_2$ resulting from the non-parametric Algorithm 1. Using $\hat{\mathbf{X}}_2(\boldsymbol{\mu}_i) = \hat{\mathbf{X}}_2$, the matrix $\mathbf{D}$ defined in (15) simplifies to

$$\mathbf{D} = [\boldsymbol{\Theta}_H \otimes \hat{\mathbf{X}}_2^T], \tag{25}$$

with $\boldsymbol{\Theta}_H$ as defined in (20). This simplified structure allows us to use preconditioning to transform the linear system (24) into a linear system for the matrix $\check{\mathbf{D}} = [\mathbf{I}_{q_H} \otimes \hat{\mathbf{X}}_2^T]$. For the monomial right-hand side $\boldsymbol{f}$ considered here, both left- and right-preconditioning are possible. For non-monomial right-hand sides $\boldsymbol{f}$, only right-preconditioning is possible as described in Appendix A. For this reason, we also present the right-preconditioning here. We substitute

$$\hat{\mathbf{O}}^T = [\boldsymbol{\Theta}_H^{-1} \otimes \mathbf{I}_{\binom{n+1}{2}}]\check{\mathbf{O}}^T \tag{26}$$

to find

$$\mathbf{D}\hat{\mathbf{O}}^T = [\boldsymbol{\Theta}_H \otimes \hat{\mathbf{X}}_2^T][\boldsymbol{\Theta}_H^{-1} \otimes \mathbf{I}_{\binom{n+1}{2}}]\check{\mathbf{O}}^T = [\mathbf{I}_{q_H} \otimes \hat{\mathbf{X}}_2^T]\check{\mathbf{O}}^T =: \check{\mathbf{D}}\check{\mathbf{O}}^T. \tag{27}$$

Then, the linear system $\check{\mathbf{D}}\check{\mathbf{O}}^T = \mathbf{R}^T$ is decoupled and can be written as

$$\hat{\mathbf{X}}_2^T\left[\check{\mathbf{H}}^{(i)}\right]^T = \hat{\hat{\mathbf{X}}}(\boldsymbol{\mu}_i)^T, \quad i = 1, \dots, q_H. \tag{28}$$

After solving for the operators $\check{\mathbf{H}}^{(i)}$, the original basis operators are then obtained via (26),

$$\hat{\mathbf{H}}^{(i)} = \sum_{j=1}^{q_H} [\boldsymbol{\Theta}_H^{-1}]_{ij}\check{\mathbf{H}}^{(j)}, \quad i = 1, \dots, q_H. \tag{29}$$

Note that this transformation involves the explicit computation of the inverse $\boldsymbol{\Theta}_H^{-1}$. This explicit computation is numerically unstable and is only possible for matrices $\boldsymbol{\Theta}_H$ with small condition number. However, the matrix $\boldsymbol{\Theta}_H$ is problem-specific and its condition number can be large. For large condition numbers, the inverse $\boldsymbol{\Theta}_H^{-1}$ should only be computed implicitly, for example via an LU or QR decomposition. For this purpose, we write the transformation (29) equivalently as linear system

$$[\boldsymbol{\Theta}_H \otimes \mathbf{I}_{\binom{n+1}{2}}]\hat{\mathbf{O}}^T = \check{\mathbf{O}}^T, \tag{30}$$

for $\hat{\mathbf{O}}^T$. This linear system is decoupled and can be written as

$$\boldsymbol{\Theta}_H\hat{\boldsymbol{o}}_{ij} = \check{\boldsymbol{o}}_{ij}, \quad i = 1, \dots, n, \; j = 1, \dots, \binom{n+1}{2} \tag{31}$$

with

$$\hat{\boldsymbol{o}}_{ij} = \begin{bmatrix} \hat{\mathbf{H}}_{ij}^{(1)} \\ \vdots \\ \hat{\mathbf{H}}_{ij}^{(q_H)} \end{bmatrix} \quad \text{and} \quad \check{\boldsymbol{o}}_{ij} = \begin{bmatrix} \check{\mathbf{H}}_{ij}^{(1)} \\ \vdots \\ \check{\mathbf{H}}_{ij}^{(q_H)} \end{bmatrix}. \tag{32}$$

The linear system (31) can be solved using standard linear algebra libraries that choose suitable solvers themselves, so these choices do not need to be made manually.

This decoupled approach is advantageous in terms of computational costs, parallelizability and numerical stability. Instead of solving the linear system (24) of dimension $sK \times q(n) = q_H\binom{n+1}{2} \times q_H\binom{n+1}{2}$ for the n columns of $\hat{\mathbf{O}}^T$, we hence solve the q_H linear systems (28) of dimension $\binom{n+1}{2} \times \binom{n+1}{2}$ for the n columns of $\left[\check{\mathbf{H}}^{(i)}\right]^T$ and the $n\binom{n+1}{2}$ linear systems (31) of dimension $q_H \times q_H$ for the vectors $\hat{\boldsymbol{o}}_{ij}$. Table 1 summarizes the computational costs of solving these three linear systems by first computing the inverse of the respective system matrix – explicitly or implicitly – and then computing the individual solutions by matrix–vector-products of the inverse and the respective right-hand-side. As can be seen, the computational costs reduce significantly from $\mathcal{O}(n^6q_H^3 + n^5q_H^2)$ for the monolithic approach to $\mathcal{O}(n^6 + n^5q_H + n^3q_H^2 + q_H^3)$ for the decoupled approach. While the monolithic system (24) can be solved in parallel for the n columns of $\hat{\mathbf{O}}^T$, the decoupled approach can be split into even more parallel jobs in two steps. First, (28) can be solved in parallel for the q_Hn columns of the operators $\left[\check{\mathbf{H}}^{(i)}\right]^T$, $i = 1, \dots, q_H$. Second, (31) can be solved in parallel for the $n\binom{n+1}{2}$ vectors $\hat{\boldsymbol{o}}_{ij}$. In terms of numerical stability, the matrix $\mathbf{D} = \boldsymbol{\Theta}_H \otimes \hat{\mathbf{X}}_2^T$ in the monolithic linear system (24) has condition number

Table 1
Summary of computational costs of solving the linear systems involved in the monolithic and decoupled approach.

	System dimension	Number of solves	Costs matrix inversion	Costs individual solutions	Total costs
Monolithic (24)	$q_H\binom{n+1}{2} \times q_H\binom{n+1}{2}$	n	$\mathcal{O}((q_H n^2)^3)$	$n \cdot \mathcal{O}((q_H n^2)^2)$	$\mathcal{O}(n^6 q_H^3 + n^5 q_H^2)$
Decoupled (28)	$\binom{n+1}{2} \times \binom{n+1}{2}$	$q_H n$	$\mathcal{O}((n^2)^3)$	$q_H n \cdot \mathcal{O}((n^2)^2)$	$\mathcal{O}(n^6 + n^5 q_H)$
Decoupled (29)	$q_H \times q_H$	$n\binom{n+1}{2}$	$\mathcal{O}(q_H^3)$	$n\binom{n+1}{2} \cdot \mathcal{O}(q_H^2)$	$\mathcal{O}(n^3 q_H^2 + q_H^3)$

$\operatorname{cond}(\mathbf{D}) = \operatorname{cond}(\boldsymbol{\Theta}_H)\operatorname{cond}(\hat{\mathbf{X}}_2^T)$, whereas the decoupled approach involves the condition numbers $\operatorname{cond}(\hat{\mathbf{X}}_2^T)$ and $\operatorname{cond}(\boldsymbol{\Theta}_H)$ separately in the linear systems (28) and (31), respectively.

As another benefit, the decoupling enables the application of methods developed for non-parametric operator inference. For example, the decoupling approach proposed in [22] can be applied to the decoupled problems (28) to reduce the computational costs and condition numbers even more.

5. Alternative derivation via Lagrange interpolation

An alternative derivation of the same decoupling approach is based on Lagrange interpolation. Concretely, [23] states that if the matrix Θ_H defined in (20) has full rank for the parameter samples $\boldsymbol{\mu}_i$, $i = 1, \dots, s$ and $s = q_H$, then we can construct alternative coefficient functions $\bar{\theta}_H^{(p)}$ such that

$$\sum_{p=1}^{q_H} \bar{\theta}_H^{(p)}(\boldsymbol{\mu})\bar{\mathbf{H}}^{(p)} = \sum_{p=1}^{q_H} \theta_H^{(p)}(\boldsymbol{\mu})\hat{\mathbf{H}}^{(p)}, \tag{33}$$

that satisfy the Lagrange property

$$\bar{\theta}_H^{(p)}(\boldsymbol{\mu}_i) = \delta_{ip}, \quad \text{for all } i, p = 1, \dots, q_H, \tag{34}$$

for the given parameter samples $\boldsymbol{\mu}_i$, with the Kronecker delta δ_{ip}.

This alternative affine decomposition (33) allows trivial decoupling of (14) since $\bar{\boldsymbol{\Theta}}_H = \mathbf{I}_s$, where $[\bar{\boldsymbol{\Theta}}_H]_{ij} = \bar{\theta}_H^{(j)}(\boldsymbol{\mu}_i)$. However, the result of this decoupled approach are the operators $\bar{\mathbf{H}}^{(i)}$, not the original ROM operators $\hat{\mathbf{H}}^{(i)}$. To compute these original operators, we combine (33) and (34) to find

$$\bar{\mathbf{H}}^{(i)} = \sum_{p=1}^{q_H} \theta_H^{(p)}(\boldsymbol{\mu}_i)\hat{\mathbf{H}}^{(p)}, \quad \text{for all } i = 1, \dots, q_H, \tag{35}$$

and can then solve for $\hat{\mathbf{H}}^{(p)}$.

Comparing the operator transformations (29) and (35), we realize that the operators $\bar{\mathbf{H}}^{(i)}$ coincide with the operators $\check{\mathbf{H}}^{((i))}$. Hence, both derivations lead to exactly the same computations. Note in particular that we do not need to compute the alternative coefficient functions $\bar{\theta}$ explicitly.

This Lagrange interpolation-based derivation does not require the snapshots $\hat{\mathbf{X}}(\boldsymbol{\mu}_i)$ to be parameter-independent. Future work should investigate whether this derivation allows decoupling also for parameter-dependent snapshots.

Note that the function $\sum_{p=1}^{q_H} \bar{\theta}_H^{(p)}(\boldsymbol{\mu})\bar{\mathbf{H}}^{(p)}$ interpolates the function values of the affine decomposition $\sum_{p=1}^{q_H} \theta_H^{(p)}(\boldsymbol{\mu})\hat{\mathbf{H}}^{(p)}$ but not necessarily those of the true parameter-dependent operator (4) if $\sum_{p=1}^{q_H} \theta_H^{(p)}(\boldsymbol{\mu})\hat{\mathbf{H}}^{(p)}$ is an approximation of (4).

6. Numerical experiments

We consider the heat equation

$$\frac{\partial}{\partial t}T(\xi, t; \boldsymbol{\mu}) = \frac{\partial}{\partial \xi}\left(\nu(T, \xi, \boldsymbol{\mu})\frac{\partial}{\partial \xi}T(\xi, t; \boldsymbol{\mu})\right) \tag{36}$$

with spatial coordinate $\xi \in \Omega = [0, 2\pi]$, time $t \in [0, 0.8]$, temperature $T : \Omega \times [0, 0.8) \to \mathbb{R}$ and two different thermal conductivities $\nu : \mathbb{R} \times \Omega \times D \to \mathbb{R}^+$ defined in Sections 6.1 and 6.2. Both conductivities have a linear temperature dependency, so the corresponding spatially-discretized FOM has the form (1) with quadratic right-hand side (2). The conductivity in Section 6.1 implies an affine decomposition (5) of the FOM operator, whereas the conductivity that will be chosen in Section 6.2 allows such a decomposition only approximately.

In both cases, we impose homogeneous Dirichlet boundary conditions

$$T(0, t) = T(2\pi, t) = 0, \quad t \in [0, 0.8], \tag{37}$$

and the initial condition

$$T(\xi, 0) = \exp(-(\xi - \pi)^2)\sin\left(\frac{\xi}{2}\right), \quad \xi \in \Omega. \tag{38}$$

Table 2
Number of linear systems of different dimensions solved during parametric operator inference for ROM dimension $n = 30$ and $q_H = 16$.

	$q_H\binom{n+1}{2} \times q_H\binom{n+1}{2}$ $= 7,440 \times 7,440$	$\binom{n+1}{2} \times \binom{n+1}{2}$ $= 465 \times 465$	$q_H \times q_H$ $= 16 \times 16$
Monolithic	$n = 30$	0	0
Decoupled	0	$\binom{n+1}{2} = 480$	$n\binom{n+1}{2} = 13,950$

We discretize with linear finite elements on an equidistant grid in space with mesh width $\Delta\xi = 2^{-7}$, and with explicit Euler in time with time step size $\Delta t = 10^{-4}$, to obtain the time-discrete dynamical system of dimension $N = 127$ for the discretized temperature $\boldsymbol{x}_k$,

$$\boldsymbol{x}_{k+1}(\boldsymbol{\mu}) = \boldsymbol{x}_k(\boldsymbol{\mu}) + \Delta t\, \mathbf{H}(\boldsymbol{\mu})\boldsymbol{x}_k^2(\boldsymbol{\mu}), \quad k = 0, \dots, K-1,\ K = 8000. \tag{39}$$

We simulate this system for both conductivities twice: first to generate snapshots to compute POD bases, then to compute snapshots for exact operator inference. The accuracy of the inferred operators is then evaluated based on the relative error with respect to the intrusive operators,

$$\frac{\left\| \sum_{p=1}^{q_H} \theta_H^{(p)}(\boldsymbol{\mu})\hat{\mathbf{H}}^{(p)} - \tilde{\mathbf{H}}(\boldsymbol{\mu}) \right\|_F}{\left\| \tilde{\mathbf{H}}(\boldsymbol{\mu}) \right\|_F}, \tag{40}$$

for specified parameter samples $\boldsymbol{\mu}$. Errors with respect to the FOM are reported in Appendix B. The code is available on https://github.com/h3rror/exactParamOpInf.

6.1. Heat equation with affine conductivity

Inspired by [8], we consider a piecewise-defined thermal conductivity but with linear temperature dependency,

$$\nu(T, \xi, \boldsymbol{\mu}) = \begin{cases} \mu_1 T & \text{for } \xi \in [0, \frac{2\pi}{16}) =: \Omega_1 \\ \vdots & \\ \mu_i T & \text{for } \xi \in [\frac{i-1}{16}2\pi, \frac{i}{16}2\pi) =: \Omega_i \\ \vdots & \\ \mu_{16} T & \text{for } \xi \in [\frac{15}{16}2\pi, 2\pi] =: \Omega_{16} \end{cases} \tag{41}$$

with parameter $\boldsymbol{\mu} \in [1, 2]^{16}$. This conductivity allows an affine decomposition of the quadratic operator,

$$\mathbf{H}(\boldsymbol{\mu}) = \sum_{p=1}^{16} \mu_p \mathbf{H}^{(p)}, \tag{42}$$

where the terms $\mathbf{H}^{(p)}$, $p = 1, \dots, 16$, correspond to the conductivity 1 in Ω_p and 0 everywhere else, respectively.

We first simulate the FOM (39) for 16 parameter samples $\bar{\boldsymbol{\mu}}_i$, $i = 1, \dots, 16$ whose entries are defined as $[\bar{\boldsymbol{\mu}}_i] = 1 + \delta_{ij}$ with the Kronecker delta δ_{ij} for all $i, j = 1, \dots, 16$. The resulting $16 \cdot (8000 + 1)$ snapshots are used to compute the global POD basis $\mathbf{V}_n \in \mathbb{R}^{N \times n}$ with $n = 1, \dots, 30$. Then we use the POD basis $\mathbf{V}_{30}$ to generate snapshot data for exact operator inference according to Algorithm 2 for the same 16 parameter samples $\boldsymbol{\mu}_i = \bar{\boldsymbol{\mu}}_i$, $i = 1, \dots, 16$. This choice of samples ensures that the matrix $\boldsymbol{\Theta}_H$ has full rank, so the solution to (14) is unique as discussed in Section 3.

Fig. 1(a) shows the errors between the inferred and the intrusive operators evaluated at $\boldsymbol{\mu}_1$, which is one of the parameter samples used in training, and $\boldsymbol{\mu}_0$, whose entries are sampled randomly from the uniform distribution in [1, 2] and which is not part of the parameter samples used in training. As can be seen, the errors are for both parameter values on the order of at most 10^{-15}, so our proposed method indeed reconstructs the intrusive operators up to machine precision. Furthermore, we cannot see any difference between the operators of the monolithic and our proposed decoupled approach. This confirms the correctness of the proposed decoupling approach. As described in Section 4, the decoupled approach has better parallelizability and significantly smaller costs. This is confirmed by Table 2, which shows the number of linear systems solved for this test case with ROM dimension $n = 30$ and $q_H = 16$. While the monolithic approach solves few very large linear systems, the decoupled approach solves many smaller systems. Consequently, the decoupled approach is much faster because the cost of solving linear systems scales cubically with their dimension. Additionally, Fig. 1(b) shows that the condition numbers of the matrices involved in the decoupled approach are smaller than the condition number of the monolithic matrix $\mathbf{D}$. Since $\boldsymbol{\Theta}_H$ is independent of the ROM dimension, $\operatorname{cond}(\boldsymbol{\Theta}_H)$ is constant. As a result, the factor by which $\operatorname{cond}(\hat{\mathbf{X}}_2^T)$ is smaller than $\operatorname{cond}(\mathbf{D})$ is also constant.

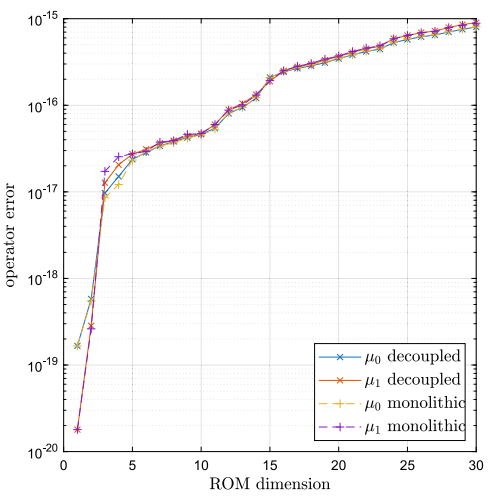

(a) Relative combined operator errors (40) evaluated at $\boldsymbol{\mu}_0$ and $\boldsymbol{\mu}_1$.

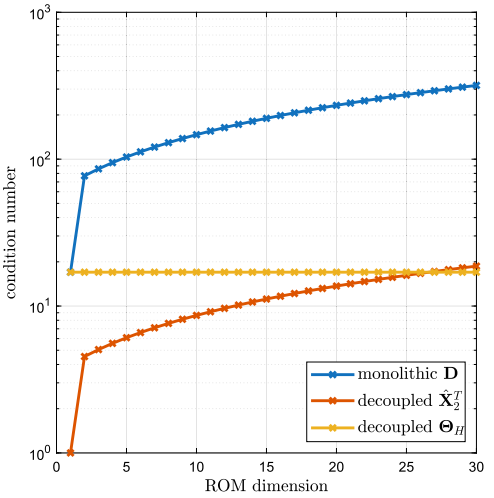

(b) Condition number of $\mathbf{D}$ for monolithic operator inference and $\hat{\mathbf{X}}_2$ and $\boldsymbol{\Theta}_H$ for decoupled operator inference.

Fig. 1. Results for the test case with affine conductivity (41).

6.2. Heat equation with non-affine conductivity

For the second test case consider, we consider the thermal conductivity

$$\nu(\xi, \mu, T) = (e^{-\frac{1}{2\pi}(\xi-\mu)^2} + 1)T, \tag{43}$$

with parameter $\mu \in \Omega$. This conductivity does not allow an exact affine decomposition of the quadratic operator. To obtain an approximate affine decomposition (5) we use a Taylor expansion of the operator $\mathbf{H}(\mu)$ with $q_H = 16$ terms,

$$\mathbf{H}(\mu) \approx \sum_{p=0}^{q_H-1} \frac{(\mu-\mu_0)^p}{p!}\mathbf{H}^{(p)}. \tag{44}$$

The expansion point μ_0 can be chosen arbitrarily, here we choose $\mu_0 = 1.3\pi$.

We first simulate the FOM (39) for 5 equidistant parameter samples in Ω, $\bar{\mu}_i = 2\pi\frac{i-1}{5-1}$, $i = 1, \dots, 5$. The resulting $5 \cdot (8000 + 1)$ snapshots are used to compute the global POD bases $\mathbf{V}_n \in \mathbb{R}^{N\times n}$ with $n = 1, \dots, 30$. Then we use the POD basis $\mathbf{V}_{30}$ to generate snapshot data for exact operator inference according to Algorithm 2 for the $q_H = 16$ equidistant parameter samples in Ω, $\mu_i = 2\pi\frac{i-1}{16-1}$, $i = 1, \dots, 16$. For this choice of samples, the matrix $\boldsymbol{\Theta}_H$ is the Vandermonde matrix of dimension 16 and has full rank, so the solution to (14) is unique as discussed in Section 3.

Fig. 2(a) shows the errors between the inferred and the intrusive operators evaluated both at the expansion point μ_0 and at $\mu_1 = 0$, which is the point in Ω with the largest distance to μ_0. As in Fig. 1(a), the errors of the decoupled and the monolithic approach do not deviate significantly from each other, so they confirm the correctness of the decoupling approach. However, compared to the previous test case depicted in Fig. 1(a), the errors for μ_0 are larger by a few orders of magnitude. This error is not associated to the accuracy of the exact operator inference approach but due to the Taylor approximation (44) used to obtain an affine decomposition. This approximation causes an inconsistency because, on the one hand, operator inference fits the $q_H = 16$ basis operators $\hat{\mathbf{H}}^{(p)}$, $p = 1, \dots, 16$ in (14) with $\theta_H^{(p)}$ defined by the Taylor approximation (44), on the other hand, the snapshot data is generated from the true FOM operator $\mathbf{H}(\mu)$. This inconsistency is demonstrated in Fig. 2(a) by the error between the intrusive ROM operators $\tilde{\mathbf{H}}^{(p)}$ corresponding to the Taylor approximation (44) computed via (6) and the true ROM operator $\tilde{\mathbf{H}}(\mu)$ computed via (4),

$$\frac{\left\|\sum_{p=1}^{q_H} \theta_H^{(p)}(\boldsymbol{\mu})\tilde{\mathbf{H}}^{(p)} - \tilde{\mathbf{H}}(\boldsymbol{\mu})\right\|_F}{\left\|\tilde{\mathbf{H}}(\boldsymbol{\mu})\right\|_F}. \tag{45}$$

As can be seen, this error ranges from 10^{-18} to 10^{-15} for all ROM dimension when evaluated at the expansion point μ_0. Indeed, the Taylor approximation (44) coincides with the true operator $\mathbf{H}(\mu)$ for this parameter value. For μ_1, however, the error ranges from 10^{-8} to 10^{-2}. Since both the true ROM operator $\tilde{\mathbf{H}}(\mu)$ and the intrusive Taylor-based ROM operators $\tilde{\mathbf{H}}^{(p)}$ are computed intrusively via projection, this error is purely due to the approximation error in the parameter space. Operator inference, on the other hand, implicitly learns a correction term $\Delta\mathbf{H}^{(p)}$ to the intrusive Taylor term, $\hat{\mathbf{H}}^{(p)} = \tilde{\mathbf{H}}^{(p)} + \Delta\mathbf{H}^{(p)}$. As can be seen, the errors of the inferred operators evaluated at μ_1 range from 10^{-20} to 10^{-15}, similarly to the errors in Fig. 1(a) where no Taylor approximation was employed. The implicit correction seems to compensate the Taylor approximation error completely. For μ_0, in contrast, the

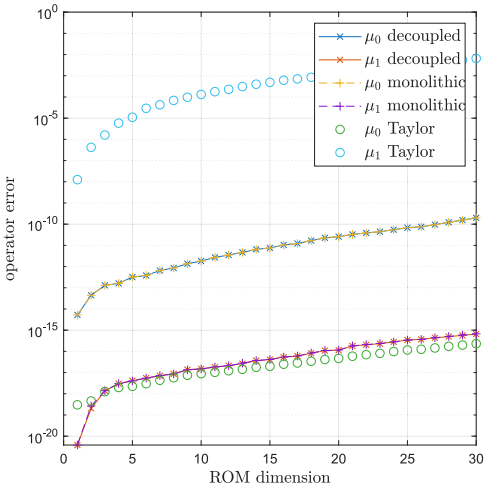

(a) Relative combined operator errors (40) and (45) evaluated at $\mu_0 = 1.3\pi$ and $\mu_1 = 0$.

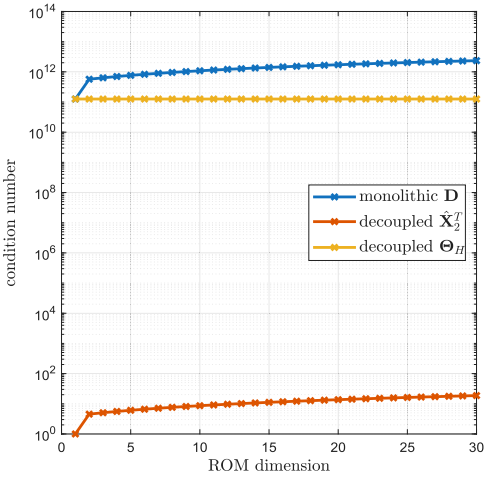

(b) Condition number of $\mathbf{D}$ for monolithic operator inference and $\hat{\mathbf{X}}_2$ and $\mathbf{\Theta}_H$ for decoupled operator inference.

Fig. 2. Results for the test case with non-affine conductivity (43).

implicit correction even deteriorates the accuracy compared to the Taylor-based ROM operators with errors ranging from 10^{-15} to 10^{-9}.

Fig. 2(b) shows again how the decoupling results in smaller conditions numbers. However, since the condition number of the Vandermonde matrix $\mathbf{\Theta}_H$ itself is very large, the benefit is relatively small here. In fact, the large condition numbers of Vandermonde matrices is limiting the choice of q_H in this test case for both monolithic and decoupled approach.

7. Conclusion

In this work, we have resolved three issues of parametric operator inference by extending our previous work on exact non-parametric operator inference, in which smartly chosen initial conditions lead to snapshot data that guarantee a full rank inference problem. First, we can guarantee the uniqueness of the operator inference solution, provided that suitable parameter samples can be found. Second, we avoid the introduction of time discretization inconsistencies and non-Markovian information that could cause errors in the inferred operators. Third, we significantly reduce the computational costs by decoupling the minimization problem.

This decoupling exploits the exact operator inference snapshot data in two steps. First, the minimization problem simplifies to a linear system. Second, this high-dimensional monolithic linear system decouples into smaller linear systems. The resulting reduction in computational costs can be decisive for the total costs of operator inference, depending on the polynomial degree and the complexity of the parameter dependency of the underlying problem and the considered ROM dimension. Furthermore, the smaller linear systems can be solved embarrassingly parallel and have a smaller condition number and are hence numerically more stable.

In numerical experiments, we demonstrate that our proposed method reconstructs intrusive parametric ROM operators up to machine precision. The experiments confirm the correctness of the decoupling approach and exemplify the improvement in condition number when replacing the monolithic system by the decoupled systems.

Future work should investigate whether the presented Lagrange interpolation-based derivation is also applicable to parameter-dependent snapshot data, as well as extensions to dynamical systems that are derived from systems of partial differential equations such as the Navier–Stokes equations.

CRediT authorship contribution statement

Henrik Rosenberger: Writing – original draft, Software, Methodology, Conceptualization. **Benjamin Sanderse:** Writing – review & editing, Funding acquisition. **Giovanni Stabile:** Writing – review & editing.

Declaration of competing interest

The authors declare that they have no known competing financial interests or personal relationships that could have appeared to influence the work reported in this paper.

Acknowledgments

This publication is part of the project "Discretize first, reduce next" (with project number VI.Vidi.193.105) of the research programme NWO Talent Programme Vidi which is (partly) financed by the Dutch Research Council (NWO). GS was funded by the European Union (ERC, DANTE, GA-101115741). Views and opinions expressed are however those of the author(s) only and do not necessarily reflect those of the European Union or the European Research Council Executive Agency. Neither the European Union nor the granting authority can be held responsible for them.

Appendix A. Decoupling for arbitrary polynomial right-hand side

The decoupling described in Section 4 can be performed analogously, if the right-hand side of (1) is any monomial in $\boldsymbol{x}$ other than quadratic. If this right-hand side consists of more than one monomial, the decoupling can be performed as follows.

A.1. Parametric dynamical system and Galerkin ROM

Let us assume that the right-hand side consists of a constant, a linear and a quadratic term,

$$\boldsymbol{f}(\boldsymbol{x};\boldsymbol{\mu}) = \boldsymbol{c}(\boldsymbol{\mu}) + \mathbf{A}(\boldsymbol{\mu})\boldsymbol{x} + \mathbf{H}(\boldsymbol{\mu})\boldsymbol{x}^2, \tag{46}$$

with operators $\boldsymbol{c}(\boldsymbol{\mu}) \in \mathbb{R}^N$, $\mathbf{A}(\boldsymbol{\mu}) \in \mathbb{R}^{N\times N}$ and $\mathbf{H}(\boldsymbol{\mu}) \in \mathbb{R}^{N\times\binom{N+1}{2}}$ with affine decompositions,

$$\boldsymbol{c}(\boldsymbol{\mu}) = \sum_{p=1}^{q_c} \theta_c^{(p)}(\boldsymbol{\mu})\boldsymbol{c}^{(p)}, \quad \mathbf{A}(\boldsymbol{\mu}) = \sum_{p=1}^{q_A} \theta_A^{(p)}(\boldsymbol{\mu})\mathbf{A}^{(p)}, \quad \mathbf{H}(\boldsymbol{\mu}) = \sum_{p=1}^{q_H} \theta_H^{(p)}(\boldsymbol{\mu})\mathbf{H}^{(p)}, \tag{47}$$

with scalar functions $\theta_c^{(p)}$, $\theta_A^{(p)}$ and $\theta_H^{(p)}$ and matrices $\boldsymbol{c}^{(p)}$, $\mathbf{A}^{(p)}$ and $\mathbf{H}^{(p)}$ of the same dimensions as $\boldsymbol{c}(\boldsymbol{\mu})$, $\mathbf{A}(\boldsymbol{\mu})$ and $\mathbf{H}(\boldsymbol{\mu})$, respectively. The intrusive ROM operators are defined as

$$\tilde{\boldsymbol{c}}(\boldsymbol{\mu}) = \mathbf{V}_n^T\boldsymbol{c}(\boldsymbol{\mu}) \in \mathbb{R}^{n\times 1}, \ \tilde{\mathbf{A}}(\boldsymbol{\mu}) = \mathbf{V}_n^T\mathbf{A}(\boldsymbol{\mu})\mathbf{V}_n \in \mathbb{R}^{n\times n} \text{ and } \tilde{\mathbf{H}}(\boldsymbol{\mu}) = \mathbf{V}_n^T\mathbf{H}(\boldsymbol{\mu})\mathbf{I}_N^{(i)}\left(\mathbf{V}_n \otimes \mathbf{V}_n\right)\mathbf{J}_n^{(i)}. \tag{48}$$

A.2. Parametric operator inference

As described in [7,9], the operator inference problem to infer the operator matrix

$$\hat{\mathbf{O}} := \left[\begin{array}{ccc|ccc|ccc} \hat{\boldsymbol{c}}^{(1)} & \cdots & \hat{\boldsymbol{c}}^{(q_c)} & \hat{\mathbf{A}}^{(1)} & \cdots & \hat{\mathbf{A}}^{(q_A)} & \hat{\mathbf{H}}^{(1)} & \cdots & \hat{\mathbf{H}}^{(q_H)} \end{array}\right] \in \mathbb{R}^{n\times q(n)}, \tag{49}$$

with $q(n) = q_c + q_A n + q_H\binom{n+1}{2}$ is then to minimize $\mathcal{L}(\hat{\mathbf{O}})$ defined in (14), but with

$$\mathbf{D} = \left[\begin{array}{c|c|c} \mathbf{D}_c & \mathbf{D}_A & \mathbf{D}_H \end{array}\right] \tag{50}$$

$$= \left[\begin{array}{c|c|c} \theta_c(\boldsymbol{\mu}_1)\otimes\mathbf{1}_K & \theta_A(\boldsymbol{\mu}_1)\otimes\hat{\mathbf{X}}(\boldsymbol{\mu}_1)^T & \theta_H(\boldsymbol{\mu}_1)\otimes\hat{\mathbf{X}}_2(\boldsymbol{\mu}_1)^T \\ \vdots & \vdots & \vdots \\ \theta_c(\boldsymbol{\mu}_s)\otimes\mathbf{1}_K & \theta_A(\boldsymbol{\mu}_s)\otimes\hat{\mathbf{X}}(\boldsymbol{\mu}_s)^T & \theta_H(\boldsymbol{\mu}_s)\otimes\hat{\mathbf{X}}_2(\boldsymbol{\mu}_s)^T \end{array}\right], \tag{51}$$

and the row vectors that encode the affine parameter dependencies in (47),

$$\boldsymbol{\theta}_c(\boldsymbol{\mu}_i) = \left[\theta_c^{(1)}(\boldsymbol{\mu}_i) \quad \cdots \quad \theta_c^{(q_c)}(\boldsymbol{\mu}_i)\right] \in \mathbb{R}^{1\times q_c} \tag{52}$$

$$\boldsymbol{\theta}_A(\boldsymbol{\mu}_i) = \left[\theta_A^{(1)}(\boldsymbol{\mu}_i) \quad \cdots \quad \theta_A^{(q_A)}(\boldsymbol{\mu}_i)\right] \in \mathbb{R}^{1\times q_A} \tag{53}$$

$$\boldsymbol{\theta}_H(\boldsymbol{\mu}_i) = \left[\theta_H^{(1)}(\boldsymbol{\mu}_i) \quad \cdots \quad \theta_H^{(q_H)}(\boldsymbol{\mu}_i)\right] \in \mathbb{R}^{1\times q_H}. \tag{54}$$

A.3. Decoupling parametric operator inference

The parametric operator inference minimization problem (14) is high-dimensional because it involves data from s parameter samples to learn q_c, q_A and q_H constant, linear and quadratic operators, respectively. We want to decouple this problem into subproblems that only involve data from one parameter sample to learn a set of one constant, one linear and one quadratic operator. For this purpose, we first note that

$$\mathcal{L}(\hat{\mathbf{O}}) = \sum_{i=1}^{s} \left\| \mathbf{D}(\boldsymbol{\mu}_i) \left[\begin{array}{c|c|c} \sum_{p=1}^{q_c} \theta_c^{(p)}(\boldsymbol{\mu}_i)\hat{\boldsymbol{c}}^{(p)} & \sum_{p=1}^{q_A} \theta_A^{(p)}(\boldsymbol{\mu}_i)\hat{\mathbf{A}}^{(p)} & \sum_{p=1}^{q_H} \theta_H^{(p)}(\boldsymbol{\mu}_i)\hat{\mathbf{H}}^{(p)} \end{array}\right]^T - \dot{\hat{\mathbf{X}}}(\boldsymbol{\mu}_i) \right\|_F^2, \tag{55}$$

with

$$\mathbf{D}^{(i)}(\boldsymbol{\mu}_i) := \left[\mathbf{1}_K \ \middle|\ \hat{\mathbf{X}}(\boldsymbol{\mu}_i) \ \middle|\ \hat{\mathbf{X}}_2(\boldsymbol{\mu}_i)\right] \in \mathbb{R}^{K\times q(n)} \quad \text{and} \quad \mathbf{1}_K = [\,1 \ \ldots \ 1\,]^T \in \mathbb{R}^K. \tag{56}$$

If $\Theta_c = \Theta_A = \Theta_H = \mathbf{I}_s$ (so $q_c = q_A = q_H = s$), then this problem simplifies to

$$\mathcal{L}(\hat{\mathbf{O}}) = \sum_{i=1}^{s} \left\| \tilde{\mathbf{D}}(\boldsymbol{\mu}_i) \left[\theta_c^{(i)}(\boldsymbol{\mu}_i)\hat{\mathbf{c}}^{(i)} \,\middle|\, \theta_A^{(i)}(\boldsymbol{\mu}_i)\hat{\mathbf{A}}^{(i)} \,\middle|\, \theta_H^{(i)}(\boldsymbol{\mu}_i)\hat{\mathbf{H}}^{(i)} \right]^T - \hat{\dot{\mathbf{X}}}(\boldsymbol{\mu}_i) \right\|_F^2, \tag{57}$$

so for all $i = 1, \dots, s$, the operators $\hat{\mathbf{c}}^{(i)}$, $\hat{\mathbf{A}}^{(i)}$, $\hat{\mathbf{H}}^{(i)}$ only depend on data from the parameter sample $\boldsymbol{\mu}_i$. Hence, we can solve subproblems for the basis operators $\hat{\mathbf{O}}^{(i)} = [\hat{\mathbf{c}}^{(i)}|\hat{\mathbf{A}}^{(i)}|\hat{\mathbf{H}}^{(i)}]$ separately.

In general, $\Theta_c = \Theta_A = \Theta_H = \mathbf{I}_s$ does not hold (i.e., we cannot find suitable parameter samples $\boldsymbol{\mu}_1, \dots \boldsymbol{\mu}_s$). However, we can achieve similar decoupling if the rank-ensuring snapshot data described in Section 3 are used and the matrices Θ_c, Θ_A and Θ_H have full rank. For this purpose, we first note that the matrices $\Theta_c \in \mathbb{R}^{s\times q_c}$, $\Theta_A \in \mathbb{R}^{s\times q_A}$ and $\Theta_H \in \mathbb{R}^{s\times q_H}$ can be extended to square full rank matrices of dimension $s \times s$. Such an extension corresponds to extending the affine expansions (5) by additional terms that evaluate to zero. Correspondingly, we extend the operator matrix $\hat{\mathbf{O}}$ to

$$\hat{\mathbf{O}} = \left[\hat{\mathbf{c}}^{(1)} \ \dots \ \hat{\mathbf{c}}^{(s)} \,\middle|\, \hat{\mathbf{A}}^{(1)} \ \dots \ \hat{\mathbf{A}}^{(s)} \,\middle|\, \hat{\mathbf{H}}^{(1)} \dots \hat{\mathbf{H}}^{(s)} \right] \in \mathbb{R}^{n\times(1+n+\binom{n+1}{2})s} \tag{58}$$

with $\hat{\mathbf{c}}^{(i)} = \mathbf{0}$ for all $i > q_c$, $\hat{\mathbf{A}}^{(i)} = \mathbf{0}$ for all $i > q_A$ and $\hat{\mathbf{H}}^{(i)} = \mathbf{0}$ for all $i > q_H$.

Next we note that the snapshot data $\hat{\dot{\mathbf{X}}}(\boldsymbol{\mu}_i) = \hat{\dot{\mathbf{X}}}$ described in Section 3 is parameter-independent, so the data matrix $\mathbf{D}$ simplifies to

$$\mathbf{D} = \left[\Theta_c \otimes \mathbf{1}_K \,\middle|\, \Theta_A \otimes \hat{\mathbf{X}}^T \,\middle|\, \Theta_H \otimes \hat{\mathbf{X}}_2^T \right]. \tag{59}$$

Now we can define

$$\check{\mathbf{O}} = \hat{\mathbf{O}}\mathbf{T}^{-T}, \quad \text{with} \quad \mathbf{T} = \begin{bmatrix} \Theta_c^{-1} \otimes \mathbf{I}_1 & & \\ & \Theta_A^{-1} \otimes \mathbf{I}_n & \\ & & \Theta_H^{-1} \otimes \mathbf{I}_{\binom{n+1}{2}} \end{bmatrix}, \tag{60}$$

then

$$\mathbf{D}\hat{\mathbf{O}}^T = \mathbf{D}\left(\check{\mathbf{O}}\mathbf{T}^T\right)^T = \mathbf{D}\mathbf{T}\check{\mathbf{O}}^T \tag{61}$$

$$= \left[\Theta_c \otimes \mathbf{1}_K \,\middle|\, \Theta_A \otimes \hat{\mathbf{X}}^T \,\middle|\, \Theta_H \otimes \hat{\mathbf{X}}_2^T \right] \begin{bmatrix} \Theta_c^{-1} \otimes \mathbf{I}_1 & & \\ & \Theta_A^{-1} \otimes \mathbf{I}_n & \\ & & \Theta_H^{-1} \otimes \mathbf{I}_{\binom{n+1}{2}} \end{bmatrix} \check{\mathbf{O}}^T \tag{62}$$

$$= \left[(\Theta_c\Theta_c^{-1}) \otimes (\mathbf{1}_K\mathbf{I}_1) \,\middle|\, (\Theta_A\Theta_A^{-1}) \otimes (\hat{\mathbf{X}}^T\mathbf{I}_n) \,\middle|\, (\Theta_H\Theta_H^{-1}) \otimes \left(\hat{\mathbf{X}}_2^T\, \mathbf{I}_{\binom{n+1}{2}}\right) \right] \check{\mathbf{O}}^T \tag{63}$$

$$= \left[\mathbf{I}_s \otimes \mathbf{1}_K \,\middle|\, \mathbf{I}_s \otimes \hat{\mathbf{X}}^T \,\middle|\, \mathbf{I}_s \otimes \hat{\mathbf{X}}_2^T \right] \check{\mathbf{O}}^T \tag{64}$$

Hence, we can decouple the problem

$$\mathcal{L}(\check{\mathbf{O}}) = \left\| \check{\mathbf{D}}\check{\mathbf{O}}^T - \mathbf{R}^T \right\|_F^2 \tag{65}$$

with $\check{\mathbf{D}} = \mathbf{D}\mathbf{T}$.

This decoupling results in smaller, embarrassingly parallel and numerically more stable subproblems

$$\mathcal{L}(\check{\mathbf{O}}^{(i)}) = \left\| \check{\mathbf{D}}^{(i)} \left(\check{\mathbf{O}}^{(i)}\right)^T - \left(\mathbf{R}^{(i)}(\boldsymbol{\mu}_i)\right)^T \right\|_F^2, \quad i = 1, \dots, s \tag{66}$$

$$\text{with } \check{\mathbf{D}}^{(i)} = \left[\mathbf{1}_K | \hat{\mathbf{X}}^T | \hat{\mathbf{X}}_2^T \right], \quad \check{\mathbf{O}}^{(i)} = [\check{\mathbf{c}}^{(i)}|\check{\mathbf{A}}^{(i)}|\check{\mathbf{H}}^{(i)}] \quad \text{and} \quad \mathbf{R}^{(i)}(\boldsymbol{\mu}_i) = \hat{\dot{\mathbf{X}}}(\boldsymbol{\mu}_i) \tag{67}$$

and facilitates extensions by new parameter samples/new parametric terms. The original operator $\hat{\mathbf{O}}$ is then computed via $\hat{\mathbf{O}} = \check{\mathbf{O}}\mathbf{T}^T$.

Note that the addition of zero terms in (58) is not necessary for exact operator inference. For example, if $q_c > q_A > q_H$, it would be sufficient to compute exact snapshot data for $\mathcal{I} = \{0, 1, 2\}$ for q_H parameter samples, for $\mathcal{I} = \{0, 1\}$ for $q_A - q_H$ samples and for $\mathcal{I} = \{0\}$ for $q_c - q_A$ samples — provided that the corresponding matrix $\mathbf{D}$ has full rank. While this approach would reduce the demand for generation of snapshot data, it would destroy the parameter independency $\hat{\dot{\mathbf{X}}}(\boldsymbol{\mu}_i) = \hat{\dot{\mathbf{X}}}$ and hence make the decoupling impossible.

Appendix B. ROM state errors with respect to the FOM

Figs. 3(a) and 3(b) show the average ROM state error with respect to the FOM,

$$\frac{\sum_{k=0}^{K} \|\boldsymbol{x}_k(\mu) - \mathbf{V}_n\tilde{\boldsymbol{x}}_k(\mu)\|_2}{\sum_{k=0}^{K} \|\boldsymbol{x}_k(\mu)\|_2}, \tag{68}$$

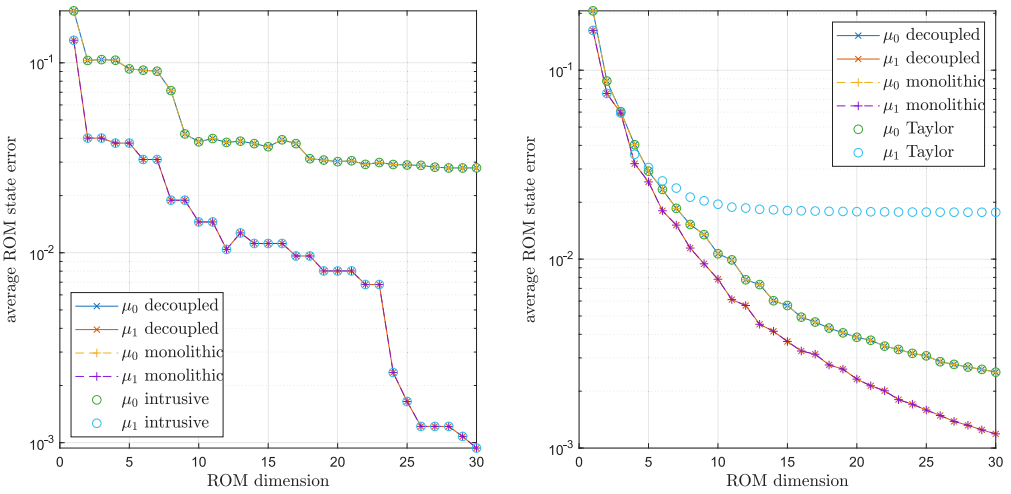

(a) Test case with affine conductivity (41). (b) Test case with non-affine conductivity (43).

Fig. 3. Relative average ROM state error.

where $\tilde{\boldsymbol{x}}_k$ are the snapshots of the explicit Euler ROM

$$\tilde{\boldsymbol{x}}_{k+1}(\boldsymbol{\mu}) = \tilde{\boldsymbol{x}}_k(\boldsymbol{\mu}) + \Delta t \left(\sum_{p=1}^{q_H} \theta_H^{(p)}(\boldsymbol{\mu}) \bar{\mathbf{H}}^{(p)} \right) \tilde{\boldsymbol{x}}_k^2(\boldsymbol{\mu}), \quad k = 0, \dots, K-1, \tag{69}$$

with the ROM operators $\bar{\mathbf{H}}^{(p)}$ computed intrusively, or via monolithic or decoupled operator inference, respectively. As can be seen in Fig. 3(a) for the affine test case, decoupled, monolithic and intrusive ROM align for both parameter values $\boldsymbol{\mu}_0$ and $\boldsymbol{\mu}_1$. The errors decrease for increasing ROM dimension, but not strictly monotonically and for $\boldsymbol{\mu}_0$ much slower than for $\boldsymbol{\mu}_1$. In Fig. 3(b) for the non-affine test case, decoupled and monolithic ROM align as well, but the Taylor-based intrusive ROM only for μ_0. This mismatch is in line with the observed mismatch of operator errors in Fig. 2(a). Also for this test case, all errors decrease with increasing ROM dimension, but for the Taylor-based intrusive ROM this decrease seems stalled for μ_1 to magnitude 10^{-2}.

Data availability

I have shared a link to my code in the manuscript.

References

[1] C. Lieberman, K. Fidkowski, K. Willcox, B. van Bloemen Waanders, Hessian-based model reduction: large-scale inversion and prediction, Internat. J. Numer. Methods Fluids 71 (2) (2013) 135–150.
[2] T. Koike, E. Qian, Energy-preserving reduced operator inference for efficient design and control, in: AIAA SCITECH 2024 Forum, 2024, http://dx.doi.org/10.2514/6.2024-1012.
[3] B. Blockmans, T. Tamarozzi, F. Naets, W. Desmet, A nonlinear parametric model reduction method for efficient gear contact simulations, Internat. J. Numer. Methods Engrg. 102 (5) (2015) 1162–1191.
[4] P. Benner, S. Gugercin, K. Willcox, A survey of projection-based model reduction methods for parametric dynamical systems, SIAM Rev. 57 (4) (2015) 483–531.
[5] B. Peherstorfer, K. Willcox, Data-driven operator inference for nonintrusive projection-based model reduction, Comput. Methods Appl. Mech. Engrg. 306 (2016) 196–215, http://dx.doi.org/10.1016/j.cma.2016.03.025, URL: https://www.sciencedirect.com/science/article/pii/S0045782516301104.
[6] B. Kramer, B. Peherstorfer, K.E. Willcox, Learning nonlinear reduced models from data with operator inference, Annu. Rev. Fluid Mech. 56 (1) (2024) 521–548.
[7] S.A. McQuarrie, P. Khodabakhshi, K.E. Willcox, Nonintrusive reduced-order models for parametric partial differential equations via data-driven operator inference, SIAM J. Sci. Comput. 45 (4) (2023) A1917–A1946.
[8] A. Vijaywargiya, S.A. McQuarrie, A. Gruber, Tensor parametric Hamiltonian operator inference, 2025, arXiv preprint arXiv:2502.10888.
[9] S. Yıldız, P. Goyal, P. Benner, B. Karasözen, Learning reduced-order dynamics for parametrized shallow water equations from data, Internat. J. Numer. Methods Fluids 93 (8) (2021) 2803–2821.
[10] I. Farcas, R. Gundevia, R. Munipalli, K.E. Willcox, Parametric non-intrusive reduced-order models via operator inference for large-scale rotating detonation engine simulations, in: AIAA Scitech 2023 Forum, 2023, p. 0172.
[11] M. Xiao, P. Breitkopf, R.F. Coelho, C. Knopf-Lenoir, P. Villon, W. Zhang, Constrained proper orthogonal decomposition based on QR-factorization for aerodynamical shape optimization, Appl. Math. Comput. 223 (2013) 254–263.
[12] B. Peherstorfer, Sampling low-dimensional Markovian dynamics for preasymptotically recovering reduced models from data with operator inference, SIAM J. Sci. Comput. 42 (5) (2020) A3489–A3515.

[13] H. Rosenberger, B. Sanderse, G. Stabile, Exact operator inference with minimal data, 2025, arXiv preprint arXiv:2506.01244.
[14] T. Bui-Thanh, K. Willcox, O. Ghattas, Parametric reduced-order models for probabilistic analysis of unsteady aerodynamic applications, AIAA J. 46 (10) (2008) 2520–2529.
[15] J. Degroote, J. Vierendeels, K. Willcox, Interpolation among reduced-order matrices to obtain parameterized models for design, optimization and probabilistic analysis, Internat. J. Numer. Methods Fluids 63 (2) (2010) 207–230.
[16] K. Carlberg, C. Farhat, J. Cortial, D. Amsallem, The GNAT method for nonlinear model reduction: effective implementation and application to computational fluid dynamics and turbulent flows, J. Comput. Phys. 242 (2013) 623–647.
[17] S. Kang, H. Kim, B. Kramer, Parametric operator inference to simulate the purging process in semiconductor manufacturing, 2025, arXiv preprint arXiv:2504.03990.
[18] H. Sharma, Z. Wang, B. Kramer, Hamiltonian operator inference: Physics-preserving learning of reduced-order models for canonical Hamiltonian systems, Phys. D: Nonlinear Phenom. 431 (2022) 133122.
[19] N. Sawant, B. Kramer, B. Peherstorfer, Physics-informed regularization and structure preservation for learning stable reduced models from data with operator inference, Comput. Methods Appl. Mech. Engrg. 404 (2023) 115836.
[20] P.d. Boef, D. Manvelyan, J. Maubach, W. Schilders, N. van de Wouw, Stable sparse operator inference for nonlinear structural dynamics, 2024, arXiv preprint arXiv:2407.21672.
[21] P. Goyal, I.P. Duff, P. Benner, Guaranteed stable quadratic models and their applications in SINDy and operator inference, 2023, arXiv preprint arXiv:2308.13819.
[22] N. Aretz, K. Willcox, Enforcing structure in data-driven reduced modeling through nested operator inference, in: 2024 IEEE 63rd Conference on Decision and Control (CDC), IEEE, 2024, pp. 8046–8053.
[23] K. Saniee, A simple expression for multivariate Lagrange interpolation, SIAM Undergrad. Res. Online 1 (1) (2008) 1–9, http://dx.doi.org/10.1137/08S010025.